Contribution from the School of Chemical Sciences, University of Illinois, Urbana, Illinois 61801, Department of Chemistry and Chemical Engineering, California Institute of Technology, Pasadena, California 91125, and Department of Chemistry, University of Virginia, Charlottesville, Virginia 22901

Magnetic Exchange Interactions in Binuclear Transition-Metal Complexes of a Binucleating Clathrochelate Ligand

MARK D. TIMKEN,[1] WILLIAM A. MARRITT,[2] DAVID N. HENDRICKSON,*[1] ROBERT A. GAGNÉ,*[2] and EKK SINN*[3]

Received December 11, 1984

A series of homo- and heterobinucleating transition-metal complexes of the form $[LM_a^{II}M_b^{II}]BF_4$ has been synthesized, where L^{3-} is the deprotonated form of a new clathrochelating ligand resulting from the Schiff-base condensation of 3 mol of 2-hydroxy-5-methylisophthalaldehyde and 2 mol of tren [tris(aminoethyl)amine]. Complexes have been prepared with the following divalent metal ions: Cu_2, Fe_2, Co_2, Mn_2, CoFe, MnFe. The binucleating nature of the ligand was established by the single-crystal X-ray structure of $[LCoFe]BF_4$, which crystallizes in the monoclinic space group Cc with a = 20.501 (10) Å, b = 11.833 (3) Å, c = 17.889 (9) Å, β = 112.44 (4)°, and Z = 4. The structure was refined by full-matrix least-squares methods to final residual values of R = 0.083 and R_w = 0.082. The cation contains both metal ions in highly distorted, six-coordinate ligand environments. The metal ions, separated by 3.07 Å, are bridged by the three deprotonated phenolic oxygens; three tren imine nitrogens complete the coordination environment. Variable-temperature (4.2-285 K) magnetic susceptibility measurements on the series of homobinuclear complexes show that the high-spin metal centers are weakly antiferromagnetically coupled. The susceptibility data for each complex were least-squares fit to the equations resultant from the spin Hamiltonian for an isotropic exchange interaction ($\hat{H} = -2J\hat{S}_1\cdot\hat{S}_2$) to give exchange parameters (J) of -33 cm^{-1} (Cu_2), -0.93 cm^{-1} (Co_2), -0.82 cm^{-1} (Fe_2), and -2.8 cm^{-1} (Mn_2). The iron-57 Mössbauer data for $[LFeMn]BF_4$ and $[LFe_2]BF_4$ are consistent with high-spin ferrous ions, although the temperature-dependent spectra (300-5.4 K) of the latter complex are unusual and suggest the presence of two inequivalent iron coordination environments.

Introduction

Robson[4] first introduced the term "binucleating ligand" in 1970 to refer to a polydentate chelating ligand that is capable of simultaneously binding two metal ions in close proximity. Quite a variety of binucleating ligands have been prepared to date.[5] Binuclear transition-metal complexes of these ligands have been studied because they have unusual physical properties, because they can serve as models of certain metalloprotein sites, because they can potentially activate small molecules such as O_2, CO, N_2, etc., and because they might serve to transport organic substrates wedged into the molecular pocket between the metal ions. A notable example of the small molecule activation is the 4e reduction of O_2 catalyzed by Co^{II}_2 derivatives of face-to-face porphyrins.[6] The interesting physical properties exhibited by the binuclear metal complexes of binucleating ligands include magnetic exchange interactions studied both by magnetic susceptibility[7] and EPR spectroscopy,[8] one-electron redox potentials resulting from metal-metal interactions,[9] and electron transfer in mixed-valence versions of these complexes.[10]

In previous papers we have used the Robson[4] macrocyclic binucleating ligand with equivalent N_2O_2 coordination sites to investigate the dependence of magnetic exchange interactions upon changes in metal ion in two series of homobinuclear complexes. In one series[11] with the Robson ligand, the divalent metal ions are five-coordinate as the result of the interaction of each metal ion with one halide ion. The antiferromagnetic exchange interaction was seen to decrease as the number of unpaired electrons increased in the series Cu(II), Ni(II), Co(II), Fe(II) to become weakly ferromagnetic in the Mn(II) complex. There was concern as to whether the metal ion coordination geometry (i.e., distance of metal ion out of the ligand plane) was changing appreciably in this series. As a consequence, the exchange interactions were also determined for a second series[12] of homobinuclear complexes of the Robson ligand where six-coordination was maintained at each metal ion by virtue of two axial ligands. The X-ray structure[12] of the Fe^{II}_2 complex showed that the six-coordinate Fe(II) ions are in the plane of the planar Robson ligand. Furthermore, the magnetic exchange interactions for this second series of six-coordinate complexes were found to be very similar to those determined for the first series with five-coordinate metal ions.

The subject of this paper is a new binucleating ligand that results from the condensation of 2 mol of tren (2,2′,2″-triaminotriethylamine) and 3 mol of 2-hydroxy-5-methylisophthalaldehyde. As can be seen in the two following illustrations of the binuclear divalent metal complexes of this clathrochelate ligand, this ligand presents an interesting, compact, and perhaps relatively inflexible environment for two metal ions.

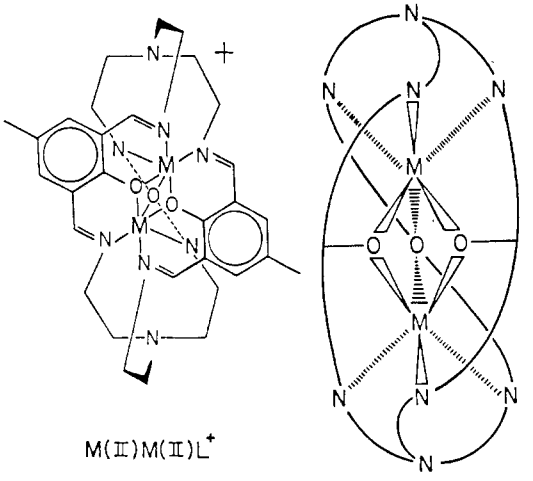

M(II)M(II)L$^+$

In the illustration on the left the third 2-hydroxy-5-methylisophthalaldehyde moiety is represented by a dotted line. As will be described in a separate paper,[13] not only can several homobinuclear metal complexes be prepared with this ligand, but several

(1) University of Illinois.
(2) California Institute of Technology.
(3) University of Virginia.
(4) Pilkington, N. H.; Robson, R. *Aust. J. Chem.* **1970**, *23*, 2225.
(5) (a) Groh, S. E. *Isr. J. Chem.* **1976/1977**, *15*, 277. (b) Nelson, S. M. *Pure Appl. Chem.* **1980**, *52*, 2461. (c) Lehn, J.-M. *Pure Appl. Chem.* **1980**, *52*, 2441.
(6) Collman, J. P.; et al. *J. Am. Chem. Soc.* **1981**, *103*, 516-33.
(7) Casellato, U.; Vigato, P. A.; Vidali, M. *Coord. Chem. Rev.* **1977**, *23*, 31.
(8) Gatteschi, D.; Bencini, A. In "Magneto-Structural Correlations in Exchange Coupled Systems"; Willett, R., Gatteschi, D., Kahn, O., Eds.; Reidel: Dordrecht, The Netherlands, 1984.
(9) (a) Hasty, E. F.; Wilson, L. J.; Hendrickson, D. N. *Inorg. Chem.* **1978**, *17*, 1835. (b) Patterson, G. S.; Holm, R. H. *Bioinorg. Chem.* **1975**, *4*, 257.
(10) Long, R. C.; Hendrickson, D. N. *J. Am. Chem. Soc.* **1983**, *105*, 1513.
(11) Lambert, S. L.; Hendrickson, D. N. *Inorg. Chem.* **1979**, *18*, 2683.
(12) Spiro, C. L.; Lambert, S. L.; Smith, T. S.; Duesler, E. N.; Gagnē, R. R.; Hendrickson, D. N. *Inorg. Chem.* **1981**, *20*, 1229.
(13) (a) Marritt, W. M. Ph.D. Thesis, California Institute of Technology, 1982. (b) Marritt, W. M.; Gagnē, R. R., manuscript in preparation.

0020-1669/85/1324-4202$01.50/0

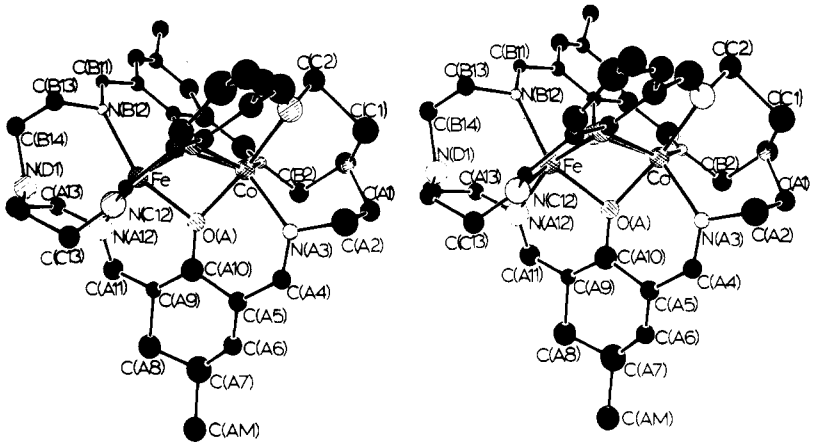

Figure 1. Stereoscopic view of the cation $[LFeCo]^+$.

heterobinuclear metal complexes are also available. In this paper the magnetic exchange characteristics of the homobinuclear Cu(II), Co(II), Fe(II), and Mn(II) complexes are described. In addition, suitable crystals of the heterobinuclear Fe(II)–Co(II) complex (BF_4^- salt) were obtained to permit an X-ray structure determination, the results of which are also given in this paper.

Experimental Section

Compound Preparation. A detailed description of the syntheses of the binuclear complexes $[LM_a^{II}M_b^{II}]BF_4$ and related compounds can be found elsewhere.[13] As such, only a brief outline of the synthesis is presented here.

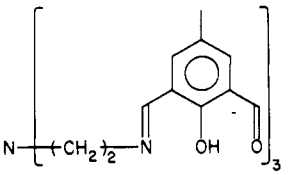

a

Precursor **a** is prepared by the reaction of tren (2,2′,2″-triaminotriethylamine) with excess 2-hydroxy-5-methylisophthalaldehyde under conditions that favor the rapid precipitation of **a**. Treatment of **a** with 1 equiv of both tren and $NaNO_3$ gives the mononuclear complex $NaLH_3NO_3$ in high yield. Upon addition of 1 equivalent of a M_a^{II} salt to a methanolic solution containing a slight molar excess of $NaLH_3NO_3$, the metal complex $LM_aH_3^{2+}$ forms almost immediately. It should be noted that for copper the insertion of an additional Cu^{II} into $LCuLH_3^{2+}$ is competitive with the initial exchange of Cu^{II} for Na^+. Consequently, preparation of the mononuclear Cu^{II} complex requires the use of an excess (2-fold) of $NaLH_3NO_3$ relative to the Cu^{II} salt. Finally, insertion of a second metal ion to form the binuclear species $[LM_a^{II}M_b^{II}]^+$ is accomplished by adding M_b^{II} salts to a solution of $LM_aH_3^{2+}$ in the presence of triethylamine. This method leads to the homobinuclear species with $M_{a,b}$ = Mn, Fe, and Co, as well as the heterobinuclear M_a = Co or Mn, M_b = Fe species. In the case of the homobinuclear copper compound, the above method yields the protonated species LCu_2H^{2+}, which can be deprotonated with diisopropylethylamine. The samples have been characterized by chemical analysis, NMR spectroscopy, and electrochemical methods described elsehwere.[13]

Physical Measurements. A PAR Model 150A vibrating-sample magnetometer, operated at 13.5 kG, was used to collect the magnetic susceptibility data on microcrystalline samples. The magnetometer was calibrated with $CuSO_4 \cdot 5H_2O$, and a calibrated GaAs diode was used for sample temperature determination and control. Diamagnetic corrections, estimated from Pascal's constants, were used in the calculation of the molar paramagnetic susceptibilities from the experimental susceptibilities. These molar susceptibilities were fit to the appropriate theoretical expressions by means of a least-squares-fitting computer program.[14]

Mössbauer (iron-57) data were collected on a previously described instrument.[15] Sample temperatures were controlled by means of a silicon diode mounted in the sample cell holder. Above 100 K, temperatures were measured with a copper–constantan thermocouple; below 100 K, with a calibrated 560-Ω Allen-Bradley resistor. Mössbauer spectra were computer fit to Lorentzian line shapes with a previously described program.[16] In all fits the areas of the two components of a quadrupole-split doublet were constrained to be equal. The isomer shifts reported are relative to that of iron foil at 298 K but are not corrected for the temperature-dependent second-order Doppler shift. The isomer shifts shown in the figures are shifted slightly; actual isomer shift data must be obtained from the tabulated data.

Powder X-ray diffraction patterns were obtained on microcrystalline samples with the use of a Norelco powder diffractometer equipped with a copper X-ray tube.

Table I. Crystal Data for $[LFeCo]BF_4$

space group: *Cc* monoclinic	
a = 20.501 (10) Å	Z = 4 (binuclear units)
b = 11.833 (3) Å	fw = 833
c = 17.889 (9) Å	ρ(calcd) = 1.38 g/cm^3
β = 112.44 (4)°	V = 4011 Å^3

Single-Crystal Data Collection and Structure Solution. Cell dimensions and space group data were obtained by standard methods on an Enraf-Nonius four-circle CAD-4 diffractometer. The θ–2θ scan technique was used, as previously described,[17] to record the intensities for all nonequivalent reflections for which $1.5° < 2\theta < 56°$. Scan widths were calculated as $(A + B \tan \theta)$, where A is estimated from the mosaicity of the crystal and B allows for the increase in peak width due to $K\alpha_1$–$K\alpha_2$ splitting. The values of A and B were found to be 0.6 and 0.35°, respectively.

The intensities of three standard reflections showed no greater fluctuations during the data collection than those expected from Poisson statistics. The raw intensity data were corrected for Lorentz–polarization and absorption. Of the 4245 independent intensities, there were 2027 with $F_o^2 > 3\sigma(F_o^2)$, where $\sigma(F_o^2)$ was estimated from counting statistics.[18] These data were used in the final refinement of the structural parameters.

A three-dimensional Patterson synthesis was used to determine the heavy-atom positions, which phased the data sufficiently well to permit location of the remaining non-hydrogen atoms from the Fourier syntheses. Full-matrix least-squares refinement was carried out as previously described.[17] Anisotropic temperature factors were introduced for metal, fluorine, oxygen, and two of the nitrogen atoms. Isotropic thermal parameters were employed for all of the other atoms. Further Fourier difference functions permitted location of 32 of the 45 hydrogen atoms; the remainder were inserted in their calculated positions. The absolute configuration was determined from comparison of the refinements of the two possible enantiomorphs. In the final stages refinements were tried where the iron and cobalt atoms were interchanged in position. This gave unusually large thermal parameters for the metal atoms and, as a consequence, suggested that the original positioning of the two metal atoms is correct. In view of the poor diffracting quality of the crystal, however,

(14) Chandler, J. P. "Program 66"; Quantum Chemistry Program Exchange, Indiana University: Bloomington, IN.
(15) (a) Cohn, M. J.; Timken, M. D.; Hendrickson, D. N. *J. Am. Chem. Soc.* **1984**, *106*, 6683. (b) Federer, W. D. Ph.D. Thesis, University of Illinois, 1984.
(16) Chrisman, B. L.; Tumolillo, T. A. *Comput. Phys. Commun.* **1971**, *2*, 322.
(17) Freyberg, D. P.; Mockler, G. M.; Sinn, E. *J. Chem. Soc., Dalton Trans.* **1976**, 447.
(18) Corfield, P. W. R.; Doedens, R. J.; Ibers, J. A. *Inorg. Chem.*, **1967**, *6*, 197.

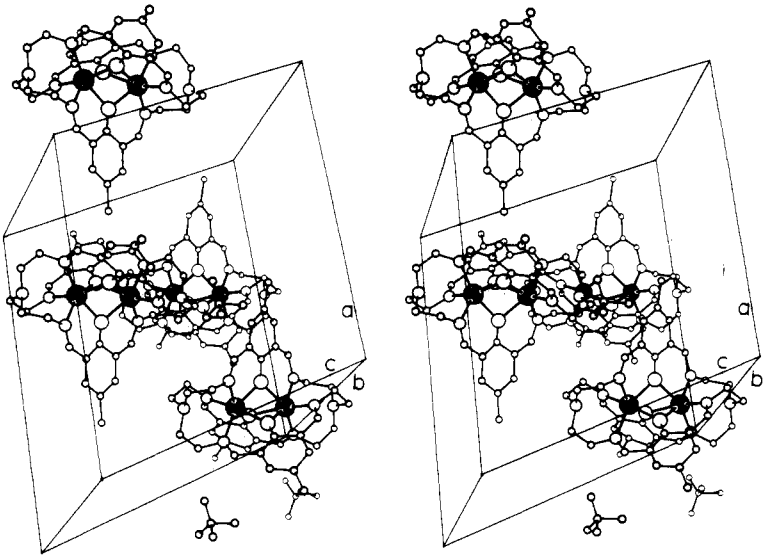

Figure 2. Stereoscopic view of the unit cell for $[LFeCo]BF_4$.

it is clear that it is difficult to distinguish between the iron and cobalt atoms.

The model converged with $R = 0.083$ and $R_w = 0.082$. A final Fourier difference map was featureless. A listing of the observed and calculated structure factors is available, together with calculated thermal parameters.[19] The principal programs used are as previously described.[17]

Results and Discussion

Molecular and Crystal Structure of $[LFeCo]BF_4$. Crystal data for $[LFeCo]BF_4$ are given in Table I. Final positional parameters for the atoms can be found in Table II, and Table III contains the most important interatomic distances and bond angles. The crystal structure consists of discrete binuclear $[LFeCo]^+$ cations and BF_4^- anions. Figure 1 shows a stereoview of the cation, while Figure 2 illustrates the ionic packing in the unit cell. As is evident from the packing diagram, the cations and anions are relatively isolated.

Although the quality of diffraction data limits the degree to which details of the cation structure can be interpreted, several important structural features are evident. The distinguishable high-spin Co^{2+} and Fe^{2+} centers are in highly distorted coordination geometries intermediate between octahedral and trigonal prismatic. It is likely that distortions are due to steric interactions within the cagelike ligand itself. Space-filling models of the ligand suggest that these interactions do not allow the cage to flex into an octahedral coordination geometry. Each metal center is bound to three imine nitrogen atoms and the three bridging oxygen atoms. The average metal–ligand bond lengths (2.22 Å for Fe–N, 2.06 Å for Fe–O, 2.14 Å for Co–N, and 2.17 Å for Co–O) are slightly different than those found for $[L'Fe_2(im)_4](BF_4)_2$ (2.08 Å for Fe–N(imine), 2.09 Å for Fe–O)[12] and $[L'Co_2Br_2]$ (2.04 Å for Co–N, 2.03 Å for Co–O),[20] where L′ is the deprotonated dianion of the planar Robson macrocycle formed from the Schiff-base condensation of 2 equiv of 1,3-propanediamine and 2 equiv of 2,6-diformyl-4-methylphenol. Intramolecular steric interactions probably account for the generally longer bonds in the L-type complex.

Structural features important for the interpretation of magnetic exchange interactions in transition-metal dimers are the metal–metal interatomic distance and the metal–bridge–metal bond angles. For $[LFeCo]BF_4$ the Fe–Co distance is 3.07 Å. The three Fe–O–Co bond angles are 92.7, 93.3, and 93.0°. Part of the motivation for this study was to compare the exchange interactions in $[LM_2]^+$ to those in $[L'M_2]^{2+}$. For $[L'Fe_2(im)_4](BF_4)_2$, which has six-coordinate Fe^{II} ions, the metal–metal distance is 3.117 Å and the bridging bond angle is 96.3°. For $[L'Co_2Br_2]$, which has square-pyramidal Co^{II} coordination geometries, the metal–metal distance is 3.158 Å and the bridge angle is 101.9°.

Although no suitable single crystals of the homobinuclear complexes $[LM_2]BF_4$ were obtained for X-ray diffraction studies, room-temperature X-ray powder patterns (see Figure 1S, Table IIIS)[19] indicate that all of the samples (including $[LFeMn]BF_4$ and $[LFeCo]BF_4$) are probably isostructural, except for the hydrated $[LCu_2]BF_4 \cdot H_2O$ sample. Even though the complexes in this series are isostructural, however, it is possible that the metal binding sites vary from dimer to dimer, since the crystal packing forces are not likely to be extremely sensitive to relatively small metal coordination geometry changes within this inflexible clathrochelate ligand.

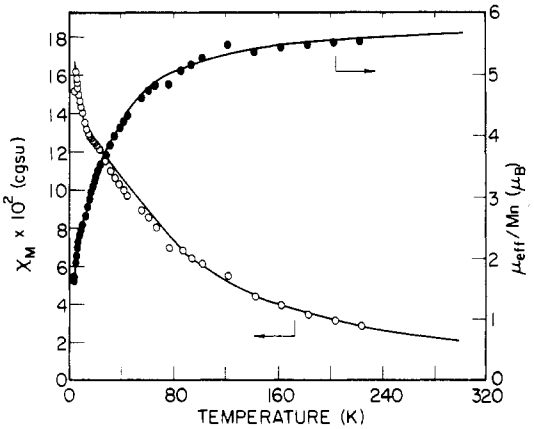

Figure 3. Molar paramagnetic susceptibility, χ_M, and effective magnetic moment, μ_{eff}/Mn, vs. temperature curves for $[LMn_2]BF_4$. The solid lines represent the least-squares fit of the data.

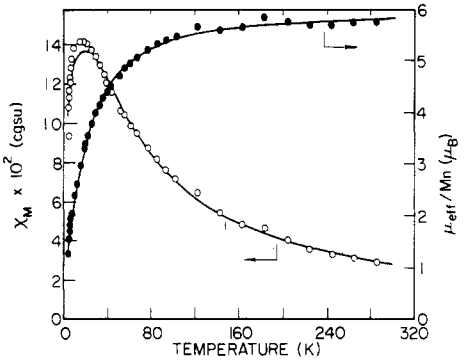

Figure 4. Molar paramagnetic susceptibility, χ_M, and effective magnetic moment, μ_{eff}/Mn, vs. temperature curves for $[LMn_2]BPh_4$. The solid lines represent the least-squares fit of the data.

(19) Supplementary material.
(20) Hoskins, B. F.; Williams, G. A. *Aust. J. Chem.* **1975**, *28*, 2607.

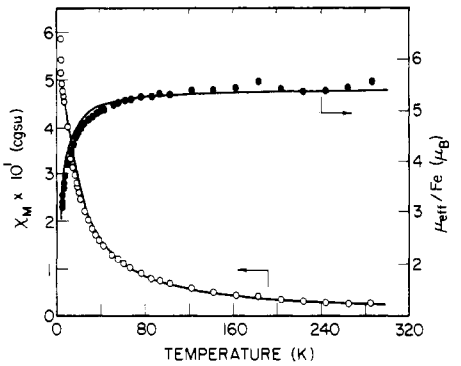

Figure 5. Molar paramagnetic susceptibility, χ_M, and effective magnetic moment, μ_{eff}/Fe, vs. temperature curves for $[LFe_2]BF_4$. The solid lines represent the least-squares fit of the data.

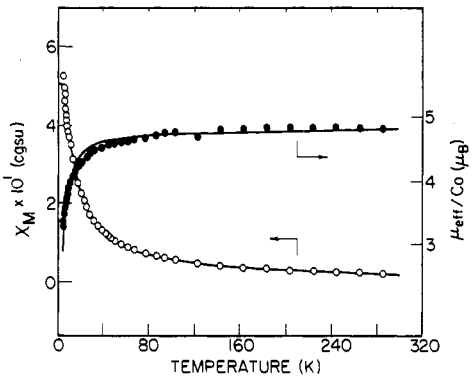

Figure 6. Molar paramagnetic susceptibility, χ_M, and effective magnetic moment, μ_{eff}/Co, vs. temperature curves for $[LCo_2]BF_4$. The solid lines represent the least-squares fit of the data.

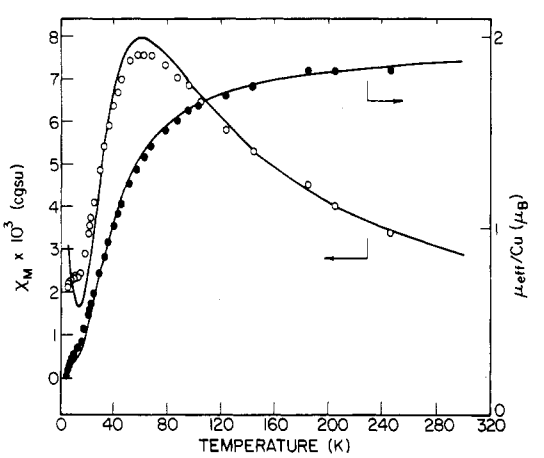

Figure 7. Molar paramagnetic susceptibility, χ_M, and effective magnetic moment, μ_{eff}/Cu, vs. temperature curves for $[LCu_2]BF_4 \cdot H_2O$. The solid lines represent the least-squares fit of the data.

Magnetic Susceptibility. The magnetic susceptibilities and magnetic moments as a function of temperature for the homobinuclear $[LM_2]^+$ salts are illustrated in Figures 3–7. In each case the magnetic moment decreases noticeably as the temperature decreases. Because of the proximity of the two metal centers in these dimers, we ascribe this magnetic behavior in large part to an *intra*molecular antiferromagnetic exchange interaction. As can be seen in Figure 2, *inter*molecular interactions that can provide pathways for an exchange interaction are not evident from the X-ray structural results. The intramolecular magnetic exchange interaction is likely propagated by the bridging oxygen atoms and not via a direct metal–metal interaction, for the intramolecular metal–metal distance is 3.07 Å.

The susceptibility data were analyzed by using a very simple model—the isotropic Heisenberg–Dirac–Van Vleck (HDVV) exchange Hamilonian, $\hat{H} = -2J\hat{S}_1 \cdot \hat{S}_2$. The theoretical magnetic

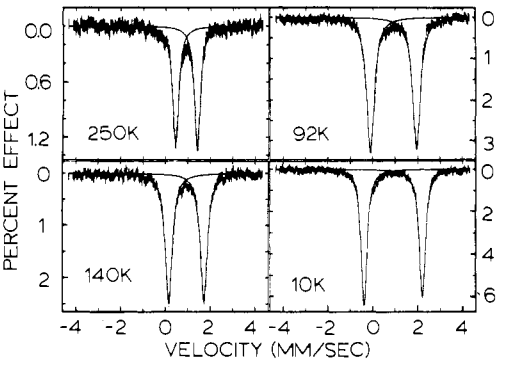

Figure 8. Variable-temperature Mössbauer spectra of $[LFeMn]BF_4$. The solid lines represent the Lorentzian line shapes that best fit the experimental data.

susceptibility expressions derived with the use of this Hamiltonian are well-known, and their descriptions can be found elsewhere.[11,21,22] Each of the dimer types, possessing a different spin S_1 ($=S_2$) value, required the use of a different theoretical susceptibility expression. In each case, the data were least-squares computer fit to the appropriate theoretical expression by varying two parameters: J, the exchange parameter in the HDVV Hamiltonian, and g, the average molecular g value. For two of the samples, $[LMn_2]BF_4$ and $[LCu_2]BF_4 \cdot H_2O$, it was necessary to include an additional term in the theoretical expression to account for the effect of a small amount of mononuclear paramagnetic impurity. The solid lines in Figures 3–7 represent the results of these fits; the numerical results are tabulated elsewhere.[19]

It is clear from the tabulated J values (Table IV) that the net exchange interaction in each dimer is antiferromagnetic and is quite weak. Only for the copper dimer does the exchange parameter exceed a few wavenumbers. Since the J values for $[LFe_2]BF_4$ and $[LCo_2]BF_4$ are very small, they have to be taken as only approximate, for single-ion, zero-field interactions may be present in these two complexes.[23] It is worthwhile to compare the J values for these complexes with those reported[11,12] for the $[L'M_2]^{2+}$ dimers, where L' is the Robson ligand described earlier. In the L' compounds, where the metal centers are bridged by two oxygen atoms, the J values increase monotonically from +0.20 cm^{-1} for $[L'Mn_2Cl_2]$ to −294 cm^{-1} for $[L'Cu_2Cl_2]$. The exchange parameter was seen to depend primarily on the total number of unpaired electrons on the metal centers and to be less dependent on the coordination geometry of the metal centers. For the L-type dimers studied in this work it is not reasonable to comment on whether or not a monotonic decrease in J with an increasing number of unpaired electrons is present. The exchange interactions are just too weak. It appears that the metal coordination and bridging geometries found in the L-type dimers either give rise to a relatively poor overlap of the magnetic orbitals on the adjacent metal centers, or enhance a ferromagnetic interaction that lowers the net antiferromagnetism. It is worth noting that for $Ni_3(acac)_6$, a linear Ni^{II} trimer in which adjacent metal centers are bridged by three acetyl oxygen atoms ($\angle$Ni–O–Ni ranges from 76.5 to 89.3°), there is a ferromagnetic interaction ($J = +26$ cm^{-1}) between adjacent nickel centers.[24] A better understanding of the magnetic exchange interactions in the $[LM_2]^{2+}$ systems will require additional X-ray structural studies of the homobinuclear complexes, as well as magnetic and structural investigations of mononuclear analogues.

Mössbauer Spectroscopy. Sufficient quantities of two of the iron-containing dimers, $[LFeMn]BF_4$ and $[LFe_2]BF_4$, were available for ^{57}Fe Mössbauer studies. This work was undertaken in order to see if the two iron centers in $[LFe_2]BF_4$ are coordinated

(21) Mabbs, F. E.; Machin, D. J. "Magnetism and Transition Metal Complexes"; Chapman and Hall: London, 1973; Chapter 7.
(22) O'Connor, C. J. *Prog. Inorg. Chem. 29*, **1982**, 203.
(23) Mulay, L. N.; Boudreaux, E. A. "Theory and Applications of Molecular Paramagnetism"; Wiley-Interscience: New York, 1976; p 198–205.
(24) Ginsberg, A. P.; Martin, R. L.; Sherwood, R. C. *Inorg. Chem.* **1968**, *7*, 932.

Table II. Positional Parameters for [LFeCo]BF_4

atom	*x*	*y*	*z*
Co	0.0	0.2499 (3)	0.25
Fe	0.0623 (3)	0.2505 (4)	0.4359 (2)
F1	−0.745 (2)	0.249 (3)	0.011 (1)
F2	−0.718 (2)	0.142 (2)	0.110 (2)
F3	−0.653 (2)	0.284 (3)	0.114 (2)
F4	−0.757 (2)	0.318 (2)	0.116 (2)
Oa	0.0383 (18)	0.373 (1)	0.3493 (17)
Ob	0.0919 (8)	0.184 (1)	0.3462 (9)
Oc	−0.0294 (11)	0.190 (2)	0.3475 (12)
N1a	−0.060 (1)	0.249 (2)	0.0650 (9)
N1d	0.124 (2)	0.255 (2)	0.6210 (16)
N3a	−0.0732 (10)	0.382 (2)	0.191 (1)
N12a	0.1429 (10)	0.379 (2)	0.494 (1)
N3b	0.0740 (10)	0.271 (2)	0.190 (1)
N12b	0.1211 (8)	0.092 (1)	0.495 (1)
N3c	−0.0507 (10)	0.102 (2)	0.193 (1)
N12c	−0.0145 (8)	0.270 (1)	0.493 (1)
C1a	−0.116 (2)	0.333 (2)	0.047 (1)
C2a	−0.1395 (15)	0.351 (3)	0.120 (2)
C4a	−0.0715 (11)	0.484 (2)	0.211 (1)
C5a	−0.0211 (12)	0.542 (2)	0.281 (1)
C6a	−0.0224 (12)	0.656 (2)	0.280 (1)
C7a	0.0390 (17)	0.721 (2)	0.341 (2)
C8a	0.0771 (13)	0.663 (2)	0.405 (2)
C9a	0.0809 (11)	0.539 (2)	0.410 (1)
C10a	0.0288 (20)	0.480 (2)	0.339 (2)
C11a	0.1368 (13)	0.487 (2)	0.473 (2)
C13a	0.2005 (12)	0.347 (2)	0.567 (1)
C14a	0.1787 (16)	0.336 (3)	0.634 (2)
CMa	0.0199 (14)	0.850 (2)	0.352 (2)
C1b	−0.0013 (11)	0.268 (2)	0.050 (1)
C2b	0.0535 (18)	0.342 (3)	0.116 (2)
C4b	0.1405 (16)	0.224 (3)	0.211 (2)
C5b	0.1698 (12)	0.151 (2)	0.279 (1)
C6b	0.2321 (14)	0.099 (2)	0.285 (2)
C7b	0.2645 (15)	0.005 (3)	0.346 (2)
C8b	0.2391 (11)	−0.000 (2)	0.404 (1)
C9b	0.1855 (9)	0.059 (2)	0.409 (1)
C10b	0.1496 (9)	0.137 (2)	0.346 (1)
C11b	0.1652 (10)	0.043 (2)	0.478 (1)
C13b	0.1124 (14)	0.054 (2)	0.572 (2)
C14b	0.1438 (17)	0.130 (3)	0.637 (2)
CMb	0.3248 (15)	−0.065 (3)	0.338 (2)
C1c	−0.0870 (13)	0.136 (2)	0.047 (2)
C2c	−0.0404 (12)	0.058 (2)	0.123 (1)
C4c	−0.0969 (14)	0.042 (2)	0.213 (2)
C5c	−0.1191 (15)	0.063 (3)	0.281 (2)
C6c	−0.1805 (14)	0.008 (3)	0.281 (2)
C7c	−0.2074 (13)	0.020 (2)	0.345 (2)
C8c	−0.1652 (11)	0.084 (2)	0.407 (1)
C9c	−0.1076 (10)	0.145 (2)	0.408 (1)
C10c	−0.0795 (15)	0.137 (3)	0.351 (2)
C11c	−0.0702 (9)	0.224 (1)	0.479 (1)
C13c	0.0091 (10)	0.346 (2)	0.566 (1)
C14c	0.0627 (16)	0.291 (3)	0.639 (2)
CMc	−0.2762 (16)	−0.029 (3)	0.341 (2)
B	−0.715 (2)	0.254 (5)	0.095 (3)
H1a	−0.094 (9)	0.41 (2)	0.04 (1)
H1′a	−0.154 (10)	0.33 (2)	−0.00 (1)
H2a	−0.162 (9)	0.29 (2)	0.13 (1)
H2′a	−0.175 (9)	0.41 (2)	0.11 (1)
H4a	−0.116 (9)	0.53 (2)	0.18 (1)
H8a	0.114 (9)	0.70 (2)	0.46 (1)
H11a	0.170 (9)	0.54 (2)	0.51 (1)
H13a	0.241 (9)	0.40 (2)	0.58 (1)
H13′a	0.219 (9)	0.27 (2)	0.55 (1)
H14a	0.168 (9)	0.40 (2)	0.66 (1)
H14′a	0.218 (9)	0.29 (2)	0.68 (1)
H1b	0.019 (9)	0.19 (2)	0.05 (1)
H1′b	−0.015 (9)	0.29 (2)	−0.00 (1)
H2b	0.039 (9)	0.42 (2)	0.13 (1)
H2′b	0.100 (9)	0.36 (2)	0.11 (1)
H4b	0.045 (9)	0.26 (2)	0.22 (1)
H6b	0.250 (9)	0.10 (2)	0.24 (1)
H8b	0.263 (9)	−0.06 (2)	0.45 (1)
H11b	0.191 (9)	−0.01 (2)	0.52 (1)
H13b	0.130 (9)	−0.01 (2)	0.59 (1)

Table II (Continued)

atom	x	y	z
H13′b	0.061 (9)	0.06 (2)	0.56 (1)
H14b	0.194 (9)	0.12 (2)	0.65 (1)
H14′b	0.129 (9)	0.10 (2)	0.68 (1)
H1c	−0.137 (9)	0.15 (2)	0.05 (1)
H1′c	−0.093 (10)	0.12 (2)	−0.01 (1)
H2c	0.010 (9)	0.06 (2)	0.13 (1)
H2′c	−0.052 (9)	−0.03 (2)	0.11 (1)
H4c	−0.116 (9)	−0.03 (2)	0.18 (1)
H6c	−0.207 (10)	−0.03 (2)	0.23 (1)
H8c	−0.179 (9)	0.10 (2)	0.45 (1)
H11c	−0.094 (9)	0.23 (2)	0.51 (1)
H13c	0.034 (9)	0.41 (2)	0.56 (1)

Table III. Bond Distances and Angles for $[LFeCo]BF_4$

	Interatomic Distances (Å)		
Co–Oa	2.20 (1)	Fe–Oa	2.04 (1)
Co–Ob	2.15 (1)	Fe–Ob	2.07 (1)
Co–Oc	2.17 (2)	Fe–Oc	2.07 (2)
Co–N3a	2.15 (1)	Fe–N12a	2.19 (1)
Co–N3b	2.19 (1)	Fe–N12b	2.26 (1)
Co–N3c	2.09 (1)	Fe–N12c	2.20 (1)
	Bond Angles (deg)		
Oa–Co–Ob	70.2 (5)	Oc–Fe–N12c	77.8 (5)
Oa–Co–Oc	71.9 (6)	N12a–Fe–N12b	100.5 (5)
Oa–Co–N3a	83.1 (5)	N12a–Fe–N12c	104.5 (5)
Oa–Co–N3b	102.8 (7)	N12b–Fe–N12c	102.7 (4)
Oa–Co–N3c	155.1 (6)	Co–Oa–Fe	92.7 (2)
Ob–Co–Oc	70.5 (5)	Co–Oa–C10a	123.6 (1)
Ob–Co–N3a	152.9 (5)	Fe–Oa–C10a	142.0 (16)
Ob–Co–N3b	82.9 (5)	Co–Ob–Fe	93.3 (4)
Ob–Co–N3c	102.0 (6)	Co–Ob–C10b	132.0 (9)
Oc–Co–N3a	106.0 (6)	Fe–Ob–C10b	133.8 (10)
Oc–Co–N3b	153.2 (6)	Co–Oc–Fe	93.0 (6)
Oc–Co–N3c	83.2 (5)	Co–Oc–C10c	135.0 (1)
N3a–Co–N3b	99.1 (6)	Fe–Oc–C10c	132.0 (2)
N3a–Co–N3c	104.2 (6)	Co–N3a–C2a	118.0 (1)
N3b–Co–N3c	99.5 (5)	Co–N3a–C4a	128.5 (1)
Oa–Fe–Ob	75.0 (6)	Fe–N12a–C11a	124.1 (1)
Oa–Fe–Oc	77.2 (7)	Fe–N12a–C13a	117.1 (10)
Oa–Fe–N12a	77.6 (5)	Co–N3b–C2b	119.3 (1)
Oa–Fe–N12b	151.2 (7)	Co–N3b–C4b	127.8 (1)
Oa–Fe–N12c	105.6 (7)	Fe–N12b–C11b	126.7 (10)
Ob–Fe–Oc	74.2 (5)	Fe–N12b–C13b	116.4 (9)
Ob–Fe–N12a	103.8 (5)	Co–N3c–C2c	121.2 (10)
Ob–Fe–N12b	77.7 (4)	Co–N3c–C4c	125.7 (1)
Ob–Fe–N12c	151.1 (5)	Fe–N12c–C11c	130.0 (10)
Oc–Fe–N12a	154.4 (7)	Fe–N12c–C13c	114.7 (7)
Oc–Fe–N12b	103.9 (6)		

Table IV. Parameters from the Fitting of Susceptibility Data to an Isotropic Exchange Hamiltonian for $[LM_2]X$

M^{2+}	Cu^{2+}	Co^{2+}	Fe^{2+}	Mn^{2+} (BF_4^-)	Mn^{2+} (PBh_4^-)
S	$^1/_2$	$^3/_2$	2	$^5/_2$	$^5/_2$
J, cm^{-1}	−33	−0.93	−0.82	−2.8	−2.3
g	2.19	2.49	2.22	1.94	2.00

equivalently by L and to determine the Mössbauer parameters for high-spin ferrous centers in the distorted coordination geometry provided by L. Both samples were examined from liquid-helium temperature up to at least 250 K.

The variable-temperature Mössbauer data for $[LFeMn]BF_4$ are illustrated in Figure 8 and Table V. This sample exhibits one quadrupole-split doublet centered at ~1.2 mm/s from 250 K down to 10 K. The isomer shift is typical for high-spin ferrous centers.[25] We can infer from these data that there is one type of coordination site in this heterobinuclear complex. The monotonic increase in the quadrupole splitting as the temperature is decreased is not atypical for high-spin ferrous molecules.[26] Such behavior is the result of changes in Boltzmann populations between

Table V. Mössbauer Effect Parameters for $[LFeMn]BF_4$

T, K	QS,[a] mm/s	IS,[a] mm/s	$\Gamma_{1/2}(-)$,[b] mm/s	$\Gamma_{1/2}(+)$,[c] mm/s
250	0.97	1.12	0.16	0.16
140	1.57	1.17	0.19	0.19
92	2.05	1.18	0.20	0.20
42	2.51	1.18	0.16	0.17
10	2.59	1.18	0.16	0.17

[a] Estimated error is 0.01 mm/s. [b] Half-width at half-height for negative velocity component. [c] Half-width at half-height for positive velocity component.

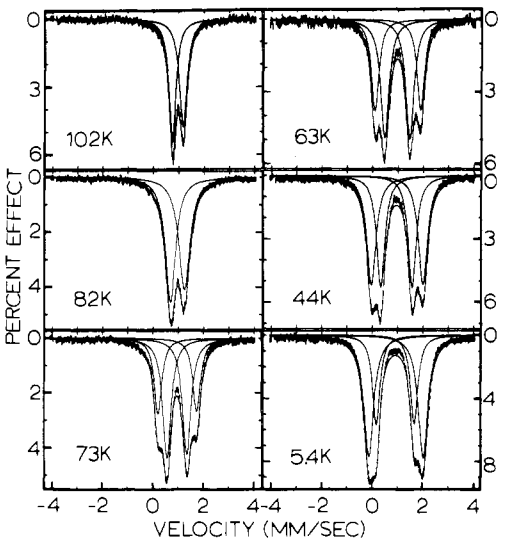

Figure 9. Variable temperature Mössbauer spectra of $[LFe_2]BF_4$. The solid lines represent the Lorentzian line shapes that best fit the experimental data.

the low-lying electronic states that form due to the low-symmetry crystal field and spin–orbit perturbations of the $^5T_2$ (O_h symmetry) electronic state. Because these states contribute differently in orientation and magnitude to the net electric field gradient (EFG) felt by the iron nucleus, changes in their relative populations will change the net EFG and the quadrupole splitting. In fact, if the sublevels of the $^5T_2$ state are equally populated, the valence contribution to the EFG is zero. In general, the total EFG experienced by the iron nucleus will depend on both the temperature-dependent valence EFG and a lattice contribution (typically temperature independent) to the EFG. The lattice EFG, which originates in the charge distribution set up by the ligand atoms and ions surrounding the iron nucleus, is generally smaller in magnitude than, and opposes, the valence EFG. For $[LFeMn]BF_4$, the three spin-quintet electronic states are apparently within thermal energy of each other, and we observe a temperature-dependent quadrupole splitting.

Mössbauer data for $[LFe_2]BF_4$ are illustrated in Figure 9 and Table VI. As with the FeMn dimer, only one quadrupole doublet centered at 1.1 mm/s is seen at high temperatures ($T \geq 82$ K). The quadrupole splitting of 0.20 mm/s at 300 K is unusually small for a high-spin ferrous center. Also unusual is the temperature dependence of the quadrupole splitting. This splitting increases slightly to a value of 0.55 mm/s at 82 K, but at ca. 73 K the

(25) Greenwood, N. N.; Gibb, T. C. "Mössbauer Spectroscopy"; Chapman and Hall: London 1971; Chapter 6.
(26) (a) Ingalls, R. *Phys. Rev. A* **1964**, *133*, 787. (b) Varret, F. *J. Phys. Colloq., Suppl. 12*, **1976**, *C6*, 437.

Table VI. Mössbauer Effect Parameters for $[LFe_2]BF_4$

T, K	QS,[a] mm/s	IS,[a] mm/s	$\Gamma_{1/2}(-)$,[b] mm/s	$\Gamma_{1/2}(+)$,[c] mm/s
300	0.20	1.08	0.12	0.13
261	0.23	1.09	0.13	0.14
130	0.37	1.08	0.15	0.17
102	0.42	1.08	0.16	0.19
82	0.55	1.08	0.24	0.27

	inner[d]					outer[e]				
T, K	QS, mm/s	IS, mm/s	area %	$\Gamma_{1/2}(-)$, mm/s	$\Gamma_{1/2}(+)$, mm/s	QS, mm/s	IS, mm/s	area %	$\Gamma_{1/2}(-)$, mm/s	$\Gamma_{1/2}(+)$, mm/s
73	0.78	1.07	64	0.20	0.21	1.53	1.09	36	0.18	0.19
63	0.99	1.07	60	0.20	0.20	1.80	1.10	40	0.18	0.18
44	1.24	1.07	48	0.19	0.19	2.03	1.10	52	0.22	0.22
23	1.42	1.07	34	0.18	0.18	2.12	1.09	66	0.25	0.25
5.4	1.50	1.06	36	0.17	0.18	2.14	1.09	64	0.23	0.23

[a] Estimated error 0.01 mm/s. [b] Half-width at half-height for negative velocity component. [c] Half-width at half-height for positive velocity component. [d] Data for inner quadrupole split doublet. [e] Data for outer quadrupole split doublet.

splitting increases dramatically and is accompanied by the appearance of two quadrupole-split doublets. The two doublets, outer and inner, continue to change in their quadrupole splittings and in their relative areas as the temperature is lowered. At 73 K the outer doublet represents only ca. 36% of the total spectral area, whereas at 5.4 K it accounts for ca. 64% of the total area. Admittedly, at 5.4 K, where the doublets overlap strongly, accurate determinations of the relative areas and quadrupole splittings are difficult. But a visual inspection of Figure 9 makes it clear that the relative areas of the inner and outer doublets do change with temperature.

These observations, although quite unusual for high-spin ferrous systems, can be rationalized in at least two ways. Any explanation, of course, must account for the unusually low quadrupole splitting at 300 K, as well as for the dramatic change in Mössbauer properties at ca. 73 K. Before we discuss possible explanations for these observations, we note that it *does not* seem possible to assign the inner doublet to site a and the outer to site b in an asymmetric dimer $[LFe_aFe_b]BF_4$. The differences in sites a and b would presumably originate in slight coordination geometry differences. The problem with this view is that although the absorption areas for sites a and b could differ due to inequalities of the recoil-free fraction f of the two sites, we would expect the absorption areas to converge as we approach 4.2 K instead of diverging as observed.

One explanation, then, for the Mössbauer behavior is that the two iron coordination sites in $[LFe_2]BF_4$ are identical, or nearly so, and that the very small quadrupole splitting at 300 K results from the thermal equilibrium among nearly equal energy electronic states of $^5T_2$ origin. The EFG (more precisely, the principal axis component of the EFG tensor) could be diminished further in magnitude by a substantial lattice EFG opposing the valence EFG. In fact, a similar explanation has been proposed[27] for $Fe(py)_4I_2$, for which the quadrupole splitting is 0.32 mm/s at 295 K. The marked spectral changes for $[LFe_2]BF_4$ at ca. 73 K could result from a structural phase transition, which gives rise to two different types of dimers, each type more distorted than the high-temperature form. Greater distortions in the coordination geometry would lead to greater energy separations of the relevant electronic states, larger valence EFG's, and larger quadrupole splittings. The incompleteness of the proposed phase transition at low temperatures is troubling, although incomplete solid-state transformations are not unknown.[28]

In a second view, both ferrous centers in a dimer are rapidly oscillating (frequency greater than ca. 10^8 s^{-1}, the Mössbauer spectroscopic time scale) between two coordination environments of nearly equal energy. If the two environments possessed EFG's with principal axes equal in magnitude, but opposite in sign, the motionally averaged EFG would be nearly spherical (i.e., zero quadrupole splitting). In this explanation, the marked changes at ca. 73 K occur when this rapid oscillation begins to "freeze-out" on the Mössbauer time scale, and the two distinct quadrupole doublets corresponding to the two coordination environments are evident. Below 73 K, slow ($<10^7$ s^{-1}) equilibrium between the two environments is maintained, with the environment represented by the outer quadrupole doublet being slightly more stable, i.e. having a more negative enthalpy than the site represented by the inner doublet.

Neither of these explanations is entirely satisfactorily in that neither really predicts the different Mössbauer characteristics of $[LFeMn]BF_4$ and $[LFe_2]BF_4$. Additional work on analogous dimers is required to understand better our observations. Nevertheless, it is clear that the clathrochelating ligand L provides an unusual coordination environment for high-spin ferrous ions.

Acknowledgment. We are grateful for support from NIH Grant HL 13652 (to D.N.H.).

Supplementary Material Available: Figure 1S, room-temperature X-ray powder patterns, and Tables IS–VIIIS, observed and calculated structure factors, thermal factors, X-ray powder data, and experimental and calculated magnetic susceptibilities and moments (18 pages). Ordering information is given on any current masthead page.

(27) Merrithew, P. B.; Rasmussen, P. G.; Vincent, D. H. *Inorg. Chem.* **1971**, *10*, 1401.

(28) (a) Nicolini, C.; Reiff, W. M. *Inorg. Chim. Acta* **1983**, *68*, 55. (b) Dockum, B. W.; Reiff, W. M. *Inorg. Chem.* **1982**, *21*, 1406.